

# Relativistic nucleon optical potentials with isospin dependence in Dirac Brueckner Hartree-Fock approach

Ruirui Xu and Zhongyu Ma

China Institute of Atomic Energy, P.O. Box 275(41), Beijing 102413, China

E. N. E. van Dalen and H. Mütter

Institut für Theoretische Physik, Universität Tübingen,  
Auf der Morgenstelle 14, D-72076 Tübingen, Germany

(Dated: November 24, 2018)

The relativistic optical model potential (OMP) for nucleon-nucleus scattering is investigated in the framework of Dirac-Brueckner-Hartree-Fock (DBHF) approach using the Bonn-B One-Boson-Exchange potential for the bare nucleon-nucleon interaction. Both real and imaginary parts of isospin-dependent nucleon self-energies in nuclear medium are derived from the DBHF approach based on the projection techniques within the subtracted  $T$ -matrix representation. The Dirac potentials as well as the corresponding Schrödinger equivalent potentials are evaluated. An improved local density approximation is employed in this analysis, where a range parameter is included to account for a finite-range correction of the nucleon-nucleon interaction. As an example the total cross sections, differential elastic scattering cross sections, analyzing powers for  $n, p + {}^{27}\text{Al}$  at incident energy  $100 \text{ keV} \leq E \leq 250 \text{ MeV}$  are calculated. The results derived from this microscopic approach of the OMP are compared to the experimental data, as well as the results obtained with a phenomenological OMP. A good agreement between the theoretical results and the measurements can be achieved for all incident energies using a constant value for the range parameter.

PACS numbers: 25.40.-h, 24.10.Jv, 24.10.Cn, 21.65.-f

## I. INTRODUCTION

The Optical Model potential (OMP) is one of the essential tools of exploring the physics of nuclear reactions. The investigations of OMP based on a fundamental microscopic theory attracts a lot of interest because it provides a reliable basis to explore nuclear reaction mechanisms in particular for cases without experimental data. With the development of radioactive beam facilities, many new physical phenomena have been and will be observed for exotic nuclei and unstable isotopes beyond the  $\beta$  stable line. A number of nuclei with large neutron excess will be produced and their structure and collisions are under investigation. Thus, the isospin dependence of the optical potentials becomes an important issue in the systematic study of OMP. However, this feature was underdeveloped for lack of direct guidance from measurements in the past. Therefore, the main purpose of this work is to construct the nucleon OMP in a microscopic way and discuss its features, especially with respect to the isospin dependence.

Different models have been used to determine a microscopic OMP [1–8]. They can be categorized as semi-phenomenological and *ab initio* approaches according to the nucleon-nucleon interaction and the approximation scheme used to describe the many-body systems. The semi-phenomenological approaches normally begin with a phenomenological nucleon-nucleon ( $NN$ ) effective interaction treated within a mean field approximation. Typical examples are the Skyrme-Hartree-Fock (SHF)[8] and the relativistic mean-field (RMF)[2]. In these approaches, the  $NN$  effective interactions are phenomeno-

logically adjusted to reproduce nuclear matter saturation properties and the ground state properties of a few well known stable nuclei. The imaginary parts of OMP are determined in an independent manner through the evaluation of the polarization diagram. On the other hand, the *ab initio* method, such as the Brueckner-Hartree-Fock (BHF)[1, 3, 7, 9] and Dirac-Brueckner-Hartree-Fock (DBHF) [5, 10–15] approaches, starts from a microscopic model of the bare  $NN$  interaction and the nuclear many-body problem is handled in a more sophisticated manner. Since the  $NN$  interaction is adjusted to describe the two-nucleon data, the many-body calculation does not contain any adjustable parameter. Therefore such studies should have a larger predictive power when applied in the study of exotic nuclear systems.

It is well known that the non-relativistic BHF fails to reproduce the empirical saturation properties of nuclear matter without an extra three-body force[7, 9]. An encouraging success has been obtained when the problem is addressed in a relativistic framework, namely the DBHF approach[10–12, 16]. The saturation properties of nuclear matter in DBHF are described rather accurately without any need to add a three-body force. Moreover, another important feature of the relativistic approach applied to finite nuclei is, that the spin-orbit potential arises naturally from the coherent sum of the contribution from the scalar and vector potentials [6], which implies that this important ingredient of OMP occurs in the DBHF treatment without the need of any adjustments.

The optical potential of a nucleon in the nuclear medium corresponds to the nucleon self-energy [17]. In the DBHF approach one can distinguish between two fre-

quently used schemes [18] to determine the relativistic components of the self-energy: the fit method versus the projection technique method. In the fit method, originally proposed by Brockmann and Machleidt [11], the scalar and vector self-energy components are directly extracted from the single particle energy. A fit to describe the momentum dependence of the single-particle energy in terms of constant scalar and vector components defines these self-energy components for each density considered. An attempt, which tries to extend this method in order to extract momentum dependent scalar and vector components by elaborate fitting procedures [19], suffers from large uncertainties. Therefore, only mean values for the self-energy components, where the explicit momentum dependence has already been averaged out, can be obtained. In symmetric nuclear matter this method turned out to be rather reliable and predicts a relativistic decomposition of the self-energy in close agreement to the analysis of the projection technique. The extension of this simple method to the isospin asymmetric nuclear matter, however, fails to determine the correct behavior of the isospin dependence of the nucleon self-energies [16, 20]. Therefore, this method is not very well suited for the construction of the microscopic OMP.

In the other method, the projection technique method, the scalar and vector components of the self-energies are directly determined from the projection onto Lorentz invariant amplitudes. These projection techniques are rather involved but more accurate. It requires the knowledge of the Lorentz structure of the positive-energy-projected in-medium on-shell  $T$ -matrix. However, ambiguities [21] arise due to the restriction to positive energy states, since pseudo-scalar ( $ps$ ) and pseudo-vector ( $pv$ ) components can not uniquely be disentangled for on-shell scattering. As a consequence an unphysical strong momentum dependence of the nucleon self-energy is obtained, when using the  $ps$  representation scheme [22]. This strong momentum dependence mainly originates from the contribution of the single  $\pi$  exchange. Therefore, it was suggested to separate the single meson exchange contributions, i.e. the bare interaction  $V$ , and the high-order corrections  $\Delta T$  [22]. The contributions of single  $\pi$  and  $\eta$  exchange are in this approach treated with the complete pseudo-vector ( $pv$ ) representation, whereas the pseudo-scalar ( $ps$ ) representation is applied only on the remaining part of  $T$ -matrix, i.e. the high-order corrections and the single meson exchanges of the other mesons. This representation scheme for the  $T$ -matrix is called the subtracted  $T$ -matrix (STM). The application of this representation scheme to the single meson exchanges reproduces the Hartree-Fock nucleon self-energies. Therefore, it is in principle equivalent to the method used in the work of Ref. [16], which not only considered symmetric nuclear matter but also pure neutron matter. This method was successfully applied to the investigation of the microscopic OMP[6] as well as the nucleus-nucleus scattering with a double folding method[23].

Recently an obvious improvement has been achieved

in the DBHF calculations using projection techniques by the extension to the general case of isospin asymmetric nuclear matter, in which the neutrons and protons are occupying different Fermi spheres [13–15]. As a consequence, one has different effective masses and self-energies for neutrons and protons. Furthermore, one has to deal with three different Pauli operators and in-medium interactions of the nucleons, to be specific the  $nn$ ,  $pp$ , and  $np$  ones. In contrast to the five independent helicity matrix elements for identical particles, six helicity matrix elements are independent in the  $np$  channel. Hence, instead of the five Lorentz invariants in the  $nn$  and  $pp$  channel, the  $T$ -matrix for the  $np$  channel is projected onto six Lorentz invariants. With this method one can obtain the real part and the imaginary part of the self-energy for symmetric and asymmetric nuclear matter.

This method has been applied in this work to investigate the isospin-dependent relativistic microscopical optical potential (RMOP). To obtain the OMP for finite nuclei, an improved local density approximation (ILDAs) method [1] is employed to determine the spacial distributions of the corresponding self-energies from the relevant density distribution and asymmetry of the finite nucleus under consideration. As an example we analyze the elastic scattering reactions of  $n, p+^{27}\text{Al}$  in terms of the RMOP and compare with experimental data and those obtained from an analysis with a phenomenological OMP.

The paper is arranged as follows. The formalism of DBHF in STM representation is briefly introduced and the nuclear matter properties with Bonn-B are described in Sec. II. In Sec. III we present the isospin-dependent RMOP and some relevant discussions. The applications of RMOP to the neutron and proton elastic scattering off  $^{27}\text{Al}$  are shown in Sec. IV. Finally, a brief summary is presented in Sec. V.

## II. DBHF APPROACH IN ASYMMETRIC NUCLEAR MATTER

### A. DBHF approach

In the relativistic DBHF scheme, the interaction between nucleons in nuclear matter is determined through the ladder approximation of the relativistic Bethe-Salpeter (BS) equation,

$$T = V + i \int V Q G G T, \quad (1)$$

where  $T$  represents the nucleon-nucleon interaction matrix in the nuclear medium and  $V$  is the bare  $NN$  interaction, respectively. The Pauli exclusion principle is included by  $Q$  operator and the in-medium nucleon propagation is introduced by the Green's function  $G$ , which fulfills the Dyson equation,

$$G = G_0 + G_0 \Sigma G. \quad (2)$$

$G_0$  denotes the free nucleon propagator, and the self-energy term  $\Sigma$  can easily be derived in first order through the following standard treatment

$$\Sigma = -i \int_F (Tr[GT] - GT), \quad (3)$$

in which the self-energy contains the direct and exchange forms at the same time, and the momentum is integrated within the Fermi sea. Because the Eqs. (1)-(3) are strongly coupled, they have to be solved iteratively until the convergence is reached.

A one boson exchange potential (OBEP) model of the bare  $NN$  interaction is normally employed for the  $V$  term in Eq. (1), and Bonn-B  $NN$  interaction is selected in this discussion. Six mesons with different ( $J^\pi, T$ ) are involved in the Bonn-B interaction, including two scalars  $\sigma$  ( $0^+, 0$ ) and  $\delta$  ( $0^+, 1$ ), two vectors  $\omega$  ( $1^-, 0$ ) and  $\rho$  ( $1^-, 1$ ), and two pseudo-vectors (pv)  $\eta$  ( $0^-, 0$ ) and  $\pi$  ( $0^-, 1$ ). For the description of isospin asymmetric nuclear matter, one needs to distinguish between protons and neutrons. Therefore, this Bonn-potential code has been made suitable to treat distinct particles in the medium [14]. As a consequence, one has three different in-medium interactions of the nucleons, to be specific the  $nn$ ,  $pp$ , and  $np$  ones. The  $np$  channel has an additional independent amplitude compared to the five independent amplitudes in the  $nn$  and  $pp$  channel.

The subtracted  $T$ -matrix (STM) representation has been applied for the projection of the  $T$ -matrix in the BS equation. The contributions of single  $\pi$  and  $\eta$  are in this approach treated with the complete pv representation. The ps representation is applied only on the remaining part of the  $T$ -matrix,

$$T_{sub} = T - V_{\pi, \eta}. \quad (4)$$

In this STM representation the ambiguity problem of the self-energy from the contributions of  $\pi$  and  $\eta$  mesons in isospin asymmetric nuclear matter can be minimized satisfactorily. Thorough discussions on generating the nucleon self-energies and comparing the reproduced bulk properties of the nuclear matter with the empirical values for the symmetric and asymmetric matter can be found in Ref. [13–15, 22].

The relativistic nucleon self-energy in the asymmetric nuclear matter is defined to satisfy the translational invariance of the homogeneous system, and its common Lorentz structure can be expressed as,

$$\Sigma^t(k, k_F, \beta) = \Sigma_s^t(k, k_F, \beta) - \gamma_0 \Sigma_0^t(k, k_F, \beta) + \boldsymbol{\gamma} \cdot \mathbf{k} \Sigma_v^t(k, k_F, \beta). \quad (5)$$

where  $\Sigma_s$  is the scalar part of self-energy,  $\Sigma_0$  and  $\Sigma_v$  denote the timelike and spacelike terms of the vector part, respectively. The superscript  $t$  is used to mark the proton and neutron, since one has to distinguish between neutrons and protons in isospin asymmetric nuclear matter. It can be seen that the self-energies are the functions of the nucleon momentum ( $k$ ), density or Fermi momentum ( $k_F$ ), and asymmetry parameter  $\beta = (\rho_n - \rho_p)/\rho$ , where  $\rho_n$ ,  $\rho_p$  and  $\rho$  indicate the neutron, proton and total densities in nuclear matter.

## B. Nucleon self-energies and nuclear matter properties

In this subsection, we present the bulk properties of nuclear matter as well as the nucleon self-energies in the DBHF approach with Bonn-B  $NN$  interaction calculated according to the procedure described in Ref. [15]. The binding energies per nucleon ( $E/A$ ) are shown in Fig. 1 as a function of the density, to be precise as a function of the corresponding Fermi momentum in symmetric nuclear matter. Various values for the asymmetry parameter  $\beta$  are considered in the range from 0.0 (symmetric matter) to 1.0 (neutron matter). The energy versus density curves do not exhibit a minimum for  $\beta \geq 0.8$ . The saturation point calculated in symmetric nuclear matter occurs at  $k_F = 1.33 \text{ fm}^{-1}$  with  $E/A = -14.71 \text{ MeV}$ . This is in good agreement with the empirical values  $k_F = 1.36 \pm 0.06 \text{ fm}^{-1}$  with  $E/A = -16 \pm 1 \text{ MeV}$ . Furthermore this figure demonstrates, that, at a given density, isospin asymmetric nuclear matter gets monotonically less attractive with increasing  $\beta$ .

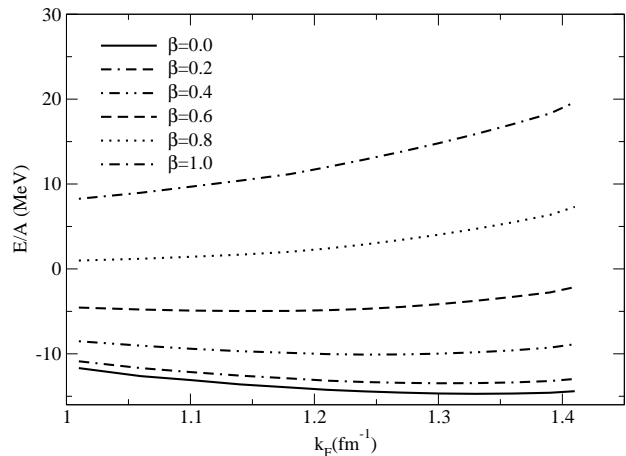


FIG. 1: Binding energy per nucleon in nuclear matter.

For the example of symmetric nuclear matter at a Fermi momentum  $k_F = 1.35 \text{ fm}^{-1}$  the real and imaginary parts of the nucleon self-energy components  $\Sigma_s$ ,  $\Sigma_0$ , and  $\Sigma_v$  are shown in Fig. 2 and Fig. 3, respectively, as functions of the on-shell nucleon energy  $E$ . This single par-

icle energy  $E$  is determined by

$$E = \sqrt{k^2(1 + \Sigma_v)^2 + (M + \Sigma_s)^2} - \Sigma_0 - M. \quad (6)$$

In these figures, one can observe that the real parts of  $\Sigma_s$  and  $\Sigma_0$  change weakly with  $E$  in Fig. 2 especially for the energies above 100 MeV. A stronger energy dependence is obtained for the imaginary parts as can be seen in Fig. 3. Note that the imaginary parts vanish at the energy  $E$  which corresponds to the Fermi energy. The real space-like part  $k\Sigma_v$  is rather small in comparison to the other two components, while the imaginary  $k\Sigma_v$  turns out to be comparable in size with  $\text{Im}\Sigma_s$ ,  $\text{Im}\Sigma_0$ .

The equivalent potential to be used in a Schrödinger equation may in a first approximation (more detailed discussion see below) be represented by the difference  $\Sigma_s - \Sigma_0$ . Hence the real parts of the self-energy components compensate each other to a large extent leading to a constant value for  $\Sigma_s - \Sigma_0$  of approximately -60 MeV for large energies  $E$ . This kind of cancellation between scalar and vector components is not observed for the imaginary part. Nevertheless also the imaginary part of  $\Sigma_s - \Sigma_0$  is essentially constant around -20 MeV at larger energies.

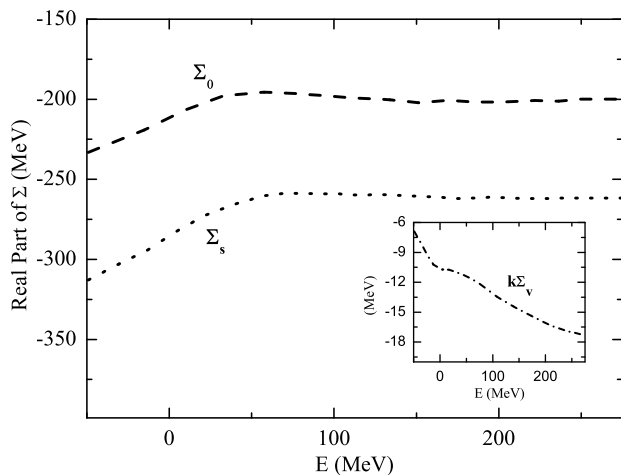


FIG. 2: Real parts of the nucleon self-energies at  $k_F=1.35 \text{ fm}^{-1}$  in symmetric nuclear matter. Note that  $k$  is the momentum of single particle.

### III. RELATIVISTIC MICROSCOPIC OPTICAL POTENTIAL IN FINITE NUCLEI

The Dirac equation of a nucleon in the nuclear medium can be written

$$[\vec{\alpha} \cdot \vec{p} + \gamma_0(M + U_s^t) + U_0^t] \Psi^t = \varepsilon \Psi^t, \quad (7)$$

where  $U_s^t$  and  $U_0^t$  are scalar and vector potentials,

$$U_s^t = \frac{\Sigma_s^t - \Sigma_v^t M}{1 + \Sigma_v^t}, \quad U_0^t = \frac{-\Sigma_0^t + \varepsilon \Sigma_v^t}{1 + \Sigma_v^t}. \quad (8)$$

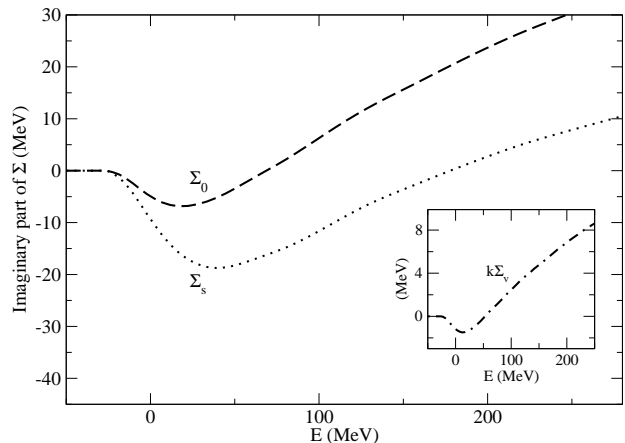


FIG. 3: Same as Fig.2, except for the imaginary parts.

and  $\varepsilon = E + M$  is the single particle energy,  $E$  is the kinetic energy of the nucleon in the free space and  $M$  indicates the mass of the nucleon.

The Dirac potentials  $U_s$  and  $U_0$  with various values for the isospin asymmetries  $\beta = 0.0, 0.2, 0.6, 1.0$  at  $k_F = 1.35 \text{ fm}^{-1}$  are plotted as functions of energies in Fig. 4. Overall, the strengths of both real and imaginary parts of scalar and vector potentials are sensitive to the asymmetry parameter in nuclear matter. The energy dependence is visibly influenced by the asymmetries for all Dirac potentials below energy  $E = 100 \text{ MeV}$ . The imaginary parts of the scalar and vector potentials are much weaker than those of the real parts. The behaviors of the imaginary parts are different from those of the real parts and their energy dependence is obviously stronger. The asymmetry dependence of the imaginary potentials for neutrons are much smaller than those for protons near the Fermi surface, but comparable at higher energies.

The optical potentials of a nucleon scattering off finite nuclei are obtained by means of the local density approximation (LDA) as usual, in which the spacial function for RMOP at the incident energy  $E$  can directly be related to the density ( $\rho$ ), momentum ( $k$ ) and asymmetry parameter ( $\beta$ ) of nuclear matter by

$$U_{LDA}(r, E) = U_{NM}(k, \rho(r), \beta), \quad (9)$$

where  $U_{LDA}$  and  $U_{NM}$  correspond to the potentials of a finite nucleus and the nuclear matter, respectively,  $\rho(r)$  is the density at nuclear radius  $r$  and related to the Fermi momentum  $k_F$  by  $\rho = (2k_F^3)/(3\pi^2)$ . To obtain the scattering amplitude and evaluate the observables for finite nuclei, a Schrödinger type equation is obtained by eliminating the lower components of the Dirac spinor in a standard way. The equation for the upper components of the wave function is transformed into

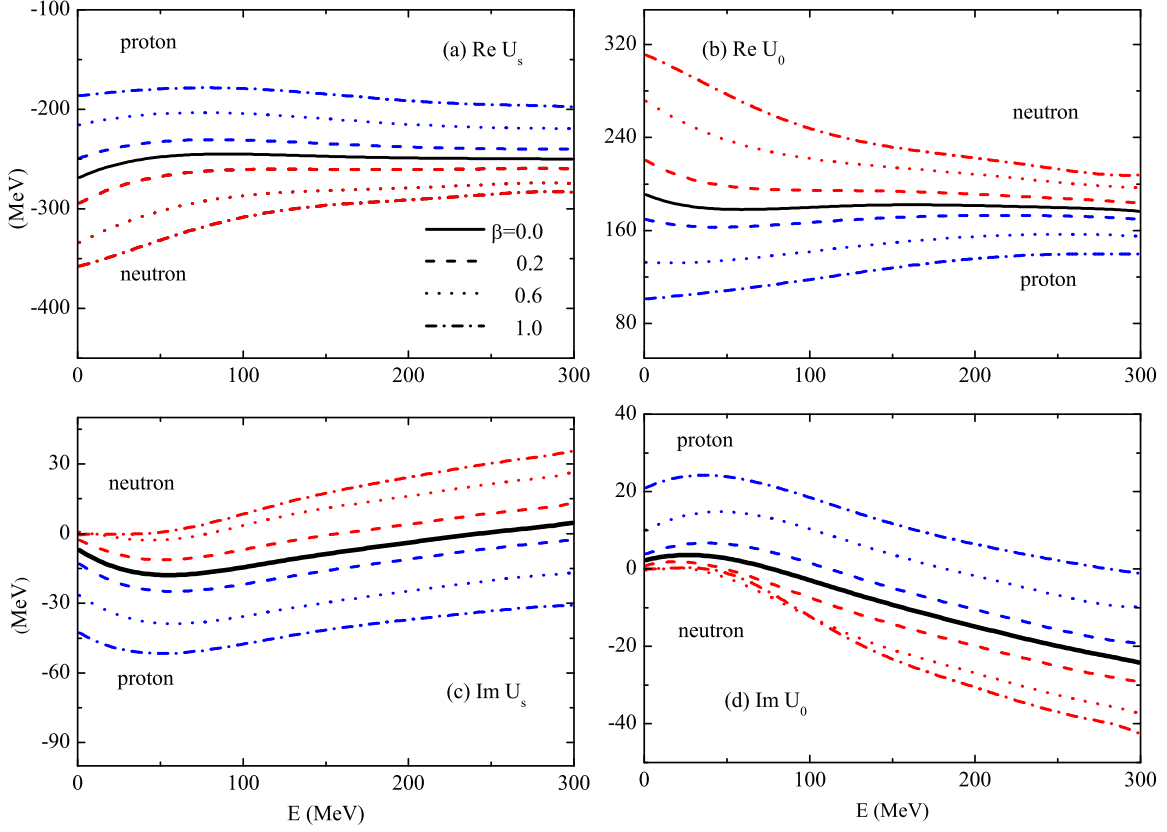


FIG. 4: (Color online) Comparison of  $U_s, U_0$  at  $k_F=1.35 \text{ fm}^{-1}$ . The real parts (upper panels) and imaginary parts (lower panels) are plotted for various  $\beta$  values. The black curves are the results for the symmetric nuclear matter, the blue curves denote those for proton and red curves for neutron.

$$\left[ -\frac{\nabla^2}{2\varepsilon} + V_{cent}^t + V_{s.o.}^t(r)\vec{\sigma} \cdot \vec{\mathbf{L}} + V_{Darwin}^t(r) \right] \varphi(\mathbf{r}) \quad (10)$$

$$= \frac{\varepsilon^2 - M^2}{2\varepsilon} \varphi(\mathbf{r}),$$

where  $V_{cent}^t$ ,  $V_{s.o.}^t$  and  $V_{Darwin}^t$  represent the Schrödinger equivalent central, spin-orbit and Darwin potentials, respectively. These potentials are related to the scalar  $U_s$  and vector  $U_0$  potentials by

$$V_{cent}^t = \frac{M}{\varepsilon} U_s^t + U_0^t + \frac{1}{2\varepsilon} [U_s^{t2} - (U_0^t + V_c)^2],$$

$$V_{s.o.}^t = -\frac{1}{2\varepsilon r D^t(r)} \frac{dD^t(r)}{dr}, \quad (11)$$

$$V_{Darwin}^t = \frac{3}{8\varepsilon D^t(r)} \left[ \frac{dD^t(r)}{dr} \right]^2 - \frac{1}{2\varepsilon r D^t(r)} \frac{dD^t}{dr} - \frac{1}{4\varepsilon D^t(r)} \frac{d^2 D^t(r)}{d^2 r},$$

where  $V_c$  is the Coulomb potential for a charged particle,  $D$  denotes a quantity defined as

$$D^t(r) = M + \varepsilon + U_s^t(r) - U_0^t(r) - V_c. \quad (12)$$

One can see again that the spin-orbit term,  $V_{s.o.}$ , emerges in a very natural way from the relativistic scheme.

Based on the Dirac potentials above, the Schrödinger equivalent potentials can be computed following Eqs. (11)-(12). Firstly, in Fig. 5, the central potential  $V_{cent}$  in the case of symmetric matter is shown as a function of incident energy at various densities, corresponding to  $k_F=1.01, 1.14, 1.24, 1.33, 1.41 \text{ fm}^{-1}$ . For this figure we dropped the Coulomb contribution to  $V_{cent}$ . It is noted that the depths of real  $V_{cent}$  decrease with increasing energy, and there is a crossing of curves for different densities around  $E = 200 \text{ MeV}$ . This implies that the so-called "wine-bottle bottom" shape appears at the the nuclear surface of finite nuclei[2]. At energies below 50 MeV the imaginary potentials  $V_{cent}$  are deepest around  $k_F = 1 \text{ fm}^{-1}$  and become weaker at higher densities. The shape of the imaginary potentials for finite nuclei contains a local maximum at the nuclear surface energies  $E < 50 \text{ MeV}$ , which indicates a surface absorption. The situation is different at energies above 75 MeV, where the absolute value of the imaginary potential increases monotonically with the density, which exhibits the behavior of volume absorption.

Additionally we compare the  $V_{cent}$  of proton and neutron versus the projectile energy  $E$  for various  $\beta$  values

at the fixed density  $k_F = 1.35 \text{ fm}^{-1}$  in Fig. 6. One finds that the depths of both real and imaginary potentials for neutrons are smaller than those for protons below  $E=250$  MeV. We specially analyze the dependence of  $V_{cent}$  on the isospin asymmetry at several energies in Fig. 7.

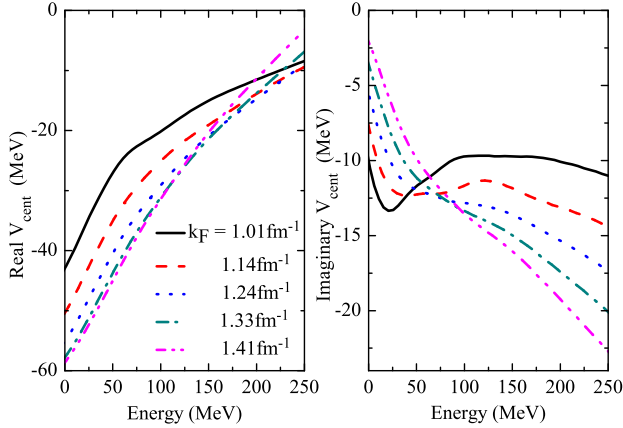


FIG. 5: (color online) The Schrödinger equivalent central potentials as functions of the incident energies in symmetric nuclear matter at the nuclear Fermi momenta  $k_F = 1.01, 1.14, 1.24, 1.33, 1.41 \text{ fm}^{-1}$ . The real and imaginary parts of  $V_{cent}$  are plotted in left and right panels, respectively.

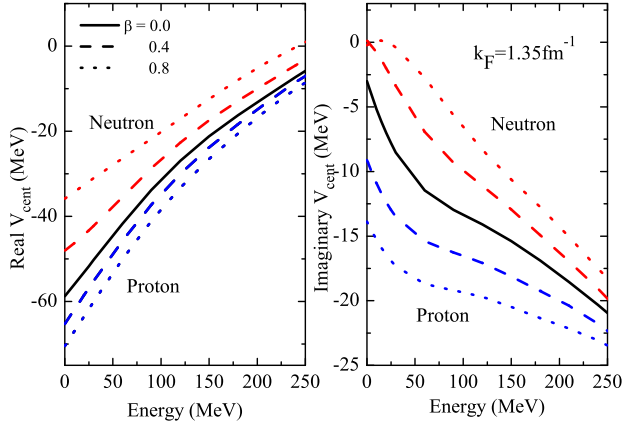


FIG. 6: (color online) The Schrödinger equivalent central potentials as functions of the incident energies in the asymmetric nuclear matter at  $k_F = 1.35 \text{ fm}^{-1}$ . The real part of  $V_{cent}$  is in the left panel. The right panel shows the imaginary part. The color notations are the same as Fig. 4.

As an example for the applications of RMOP we study the experimental scattering data for the nucleon scattering off aluminum targets. An empirical formula by Negele [24] is employed to generate the nucleon density distribution of the stable  $^{27}\text{Al}$  and two unstable neutron-rich isotopes  $^{37,47}\text{Al}$ , as shown in Fig. 8. The asymmetry is assumed constant in the interior of nucleus and determined by  $\beta = (N - Z)/A$ , where  $N, Z, A$  indicate the numbers of neutron, proton and total nucleons of a finite nucleus. Thus, the asymmetries of  $^{27,37,47}\text{Al}$  are respec-

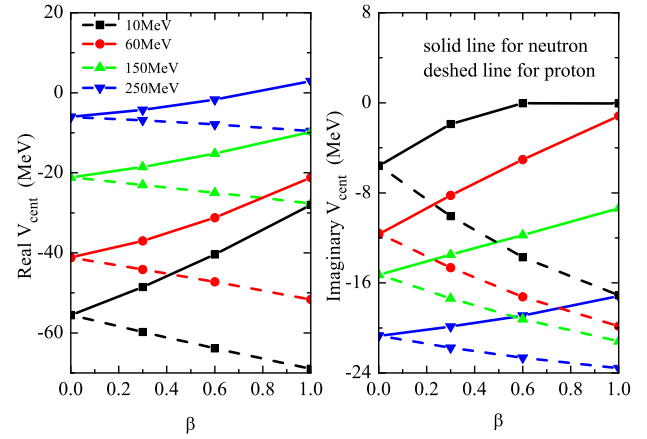


FIG. 7: (Color online) The central potentials as functions of asymmetry  $\beta$  at  $k_F = 1.35 \text{ fm}^{-1}$ . The black, red, green and blue ones correspond to the incident energies  $E = 10, 60, 150, 250$  MeV, respectively. Solid curves are for neutron and dashed ones for proton.

tively taken as 0.037, 0.297 and 0.447.

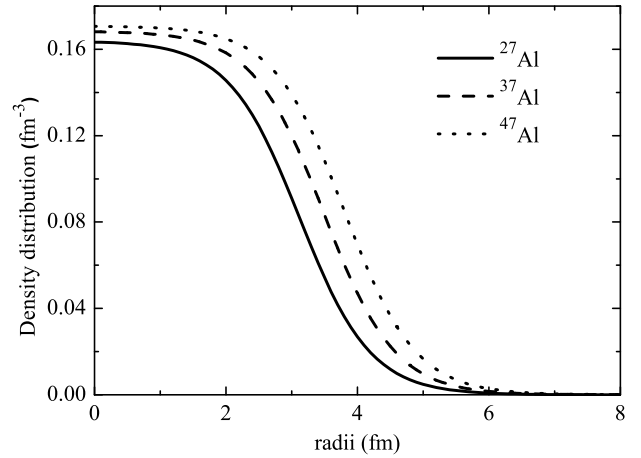


FIG. 8: Nucleon densities of  $^{27}\text{Al}$  and two unstable isotopes  $^{37,47}\text{Al}$

In this discussion, we adopt the finite range correction with Gaussian form to make modifications in the potentials via LDA approach, namely improved local density approximation (ILDAs)[1]. The potential  $U_{ILDA}$  of the finite nucleus is finally obtained through the following integral,

$$U_{ILDA}(r, E) = (t\sqrt{\pi})^{-3} \times \int U_{LDA}(r', E) \exp(-|\vec{r} - \vec{r}'|^2/t^2) d^3r', \quad (13)$$

where  $t$  is the parameter, that represents the effective range of  $U_{LDA}$  at radius  $r'$ . This is the only adjusted parameter in this calculation and is selected as a constant 1.4 fm in all cases.

We derive the Schrödinger equivalent potentials,  $V_{cent}^t$ ,  $V_{s.o.}^t$ ,  $V_{Darwin}^t$ , for  $n, p+^{27,37,47}\text{Al}$  through this ILDA ap-

proach. The potentials of neutron scattered from the stable  $^{27}\text{Al}$  at  $E = 10, 150, 250$  MeV are plotted in Fig. 9. The depths of the real potentials decrease as the energy increases and the imaginary parts change from the surface absorption to the volume absorption. These behaviors are consistent with the phenomenological OMP. It can also be observed that the main contribution of RMOP comes from the central potential  $V_{cent}$ , the spin-orbit  $V_{s.o.}$  and Darwin  $V_{Darwin}$  terms are the necessary supplements to the central potential. In Fig. 10, we construct the  $V_{cent}$ , for neutron scattered from  $^{27}\text{Al}$  and the neutron-rich  $^{37,47}\text{Al}$ . Due to the varying nucleon density distributions and asymmetries, the depths of  $V_{cent}$  of the Al isotopes become smaller in the interior of the nuclei ( $r < 3$  fm) with the increasing neutron numbers, while the potentials of heavier nuclei are expanded for a large radius. Meanwhile, we analyze  $V_{cent}$  of  $n+^{47}\text{Al}$  at  $E = 150$  MeV in Fig. 11 to check the impact of isospin asymmetry on the potential. It is found that the central potentials of  $^{47}\text{Al}$  are clearly affected by the isospin inside the nucleus. The impact is believed to become stronger for those nuclei with larger values for  $\beta$ .

#### IV. RESULTS AND DISCUSSION

In this section, we discuss the angular distributions and analyzing powers of  $n, p+^{27}\text{Al}$  and the cross sections of  $^{27}\text{Al}(n, \text{tot})$  at  $100 \text{ keV} < E < 250$  MeV. At very low energies the elastic scattering from the compound nucleus is sizable in addition to those from the OMP. In order to compare with the experimental data the Hauser-Feshbach model is utilized to determine the contribution from the compound nucleus. For a particular incident energy, there are six open single particle emission channels from the compound nucleus, including the neutron, proton, deuteron, tritium,  $\alpha$ , Helium-3 channels. The first several discrete states are taken as the competing channels. For higher excitation energies, a continuum described by the GilbertCCameron level density formula[25] is provided as compensation. Therefore, the computed observables contain the contributions from both shape and compound elastic scattering processes. All calculations mentioned above are performed with the assistance of the APMN code[26].

The present calculations are systematically compared with the experimental data and the results obtained with the global phenomenological OMP, Koning-Delaroche (KD) potential [27] in Figs. 12-15. The experimental data in these figures, the total cross sections  $\sigma_{tot}$ , the differential elastic scattering cross sections  $d\sigma/d\Omega$  and the analyzing powers  $A_y(\theta)$ , are assembled in Table I - II. The calculated observables of the neutron and proton induced reactions are both in good agreement with experimental data. Moreover, the results of the RMOP are very similar to those with the global KD potential. In some energy regions our predictions are even better than those with the phenomenological ones, such as the

TABLE I:  $\sigma_{tot}$ ,  $d\sigma/d\Omega$  and  $A_y(\theta)$  database for  $n+^{27}\text{Al}$

Data	Ref.	Energy(MeV)
$\sigma_{tot}$	[28]	0.25 - 27.0
	[29]	5.3 - 250.0
$d\sigma/d\Omega$	[30]	2.0 - 80.1
	[31]	3.2
	[32]	5.4, 6.4, 7.5, 8.6
	[33]	7.6
	[34]	10.9, 13.9, 16.9
	[35]	15.4
	[36]	18.0, 20.0, 22.0, 25.0, 26.0
	[37]	84.0
	[38]	96.0
	[39]	136.0
$A_y(\theta)$	[33]	7.6
	[40]	14.0, 17.0
	[35]	15.4

TABLE II:  $d\sigma/d\Omega$  and  $A_y(\theta)$  database for  $p+^{27}\text{Al}$

Data	Ref.	Energy(MeV)
$d\sigma/d\Omega$	[41]	0.8, 1.0, 2.0, 3.0
	[42]	17.0
	[43]	17.5
	[44]	28.0
	[45]	61.4
	[46]	92.9, 95.7
	[47]	142.0
	[48]	156.0
	[49, 50]	160.0, 177.0, 183.0
$A_y(\theta)$	[51]	185.0
	[52]	13.7, 15.0, 17.0, 19.0, 21.0, 23.0, 25.0

angular distributions of  $p+^{27}\text{Al}$  at  $E > 95.7$  MeV in Fig. 13. As a conclusion, it is proved that the present RMOP based on the DBHF approach is suitable to describe the potentials of  $n, p+^{27}\text{Al}$ , especially for the spin-orbit term  $V_{s.o.}$ , which is validated through the apparent agreement to the measured analyzing power data in Fig. 14.

We particularly investigate the DBHF central potential of  $n+^{27}\text{Al}$  at  $E = 150$  MeV with the ILDA approach and the conventional LDA approach in Fig. 16. The  $V_{cent}$  of the phenomenological KD model is also displayed in this figure. It is observed that the depths of the real and imaginary  $V_{cent}$  in LDA method are obviously deeper and exhibit a smaller range than those of the KD potentials. This differences are reduced after the finite range corrections in ILDA approach are taken into account, and the corresponding RMOP looks closer to KD ones. Therefore, rather similar scattering results in Figs. 12-15 are obtained with both potentials.

#### V. SUMMARY

In this work, we study the RMOP for finite nuclei in the framework of the DBHF approach with projection

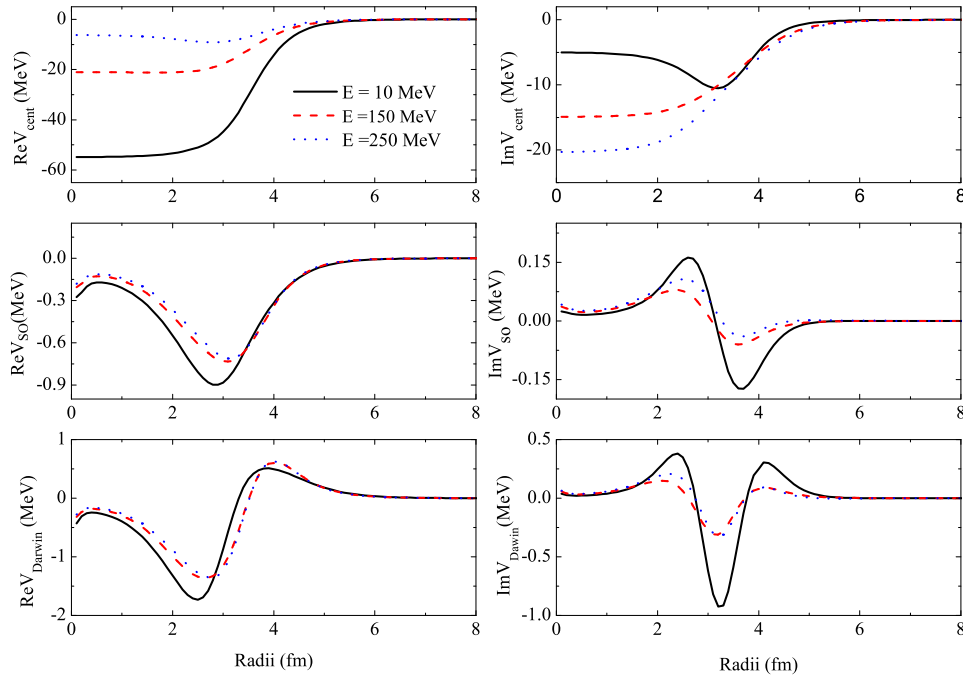


FIG. 9: (Color online) The Schrödinger equivalent central, spin-orbit and Darwin potentials as functions of radius for  $n+^{27}\text{Al}$  at  $E=10, 150, 250$  MeV.

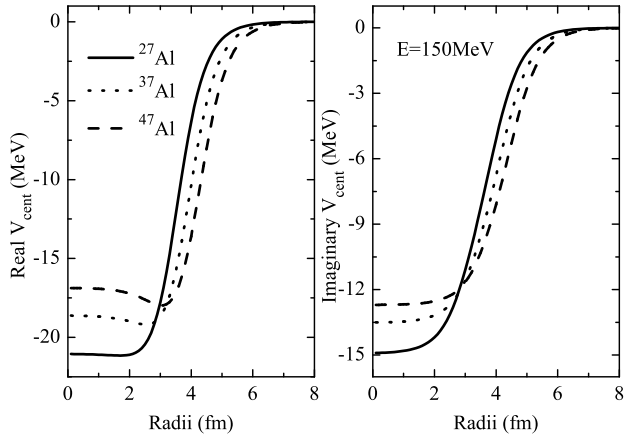


FIG. 10: The  $V_{cent}$  of  $n+^{27,37,47}\text{Al}$  at  $E=150$  MeV. The real parts are shown in the left and the imaginary ones in the right.

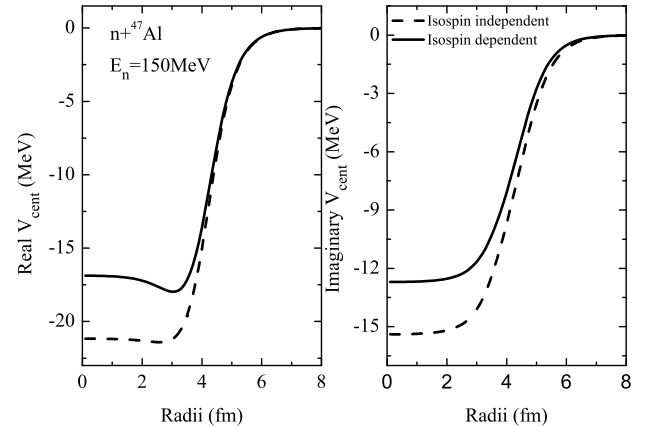


FIG. 11: The  $V_{cent}$  of  $n+^{47}\text{Al}$  in the isospin dependent mode and those for neglecting the isospin asymmetry at  $E=150$  MeV. The left panel shows the real parts, the right one for the imaginary parts.

techniques using the Bonn-B bare  $NN$  interactions. Special attention is paid to the isospin dependence. The subtracted  $T$ -matrix representation is applied to minimize the ambiguities, which arise due to the restriction to positive energy states in the DBHF approach, in the determination of the nucleon self-energies for isospin asymmetric nuclear matter. In this way the precise form of the nucleon self-energies with its momentum and isospin dependence are determined. Thus, the nucleon RMOP is obtained from the results of these DBHF calculations. An ILDA method is adopted to intimately relate the density and isospin dependence of the RMOP in nuclear mat-

ter to the radial dependence in finite nuclei. A widely used empirical density distribution is employed for finite nuclei. Only one free parameter in ILDA is adapted in RMOP, which is fixed to be  $t=1.4$  fm for all calculations.

As an example of the applications we investigate the elastic scattering of  $n, p+^{27}\text{Al}$  at  $100 \text{ keV} < E < 250$  MeV. The predicted observables in this approach are compared with experimental data and with results from phenomenological KD potentials. Good agreement is obtained. In addition, we perform a first analysis of the RMOP for the unstable neutron-rich nuclei  $^{37,47}\text{Al}$ . It is



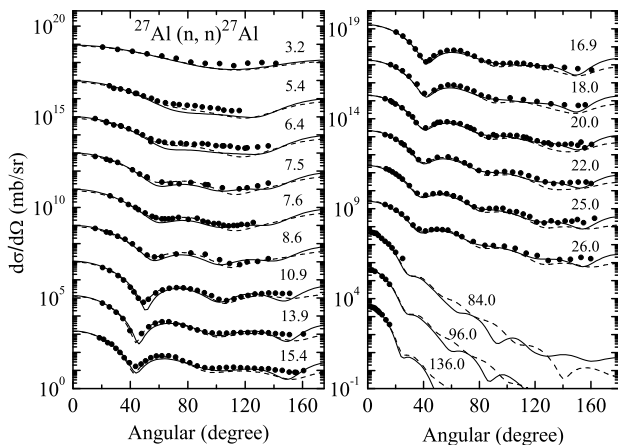


FIG. 12: Angular distributions of  $n+^{27}\text{Al}$  elastic scattering at  $3.2 \text{ MeV} < E < 136 \text{ MeV}$ . The curves and data points at the bottom represent their true values, the others are multiplied by factors of  $10^2$ ,  $10^4$ , etc. The solid curves and dashed ones indicate the results calculated with RMOP and KD potentials, respectively. The dots are experimental data listed in Table I.

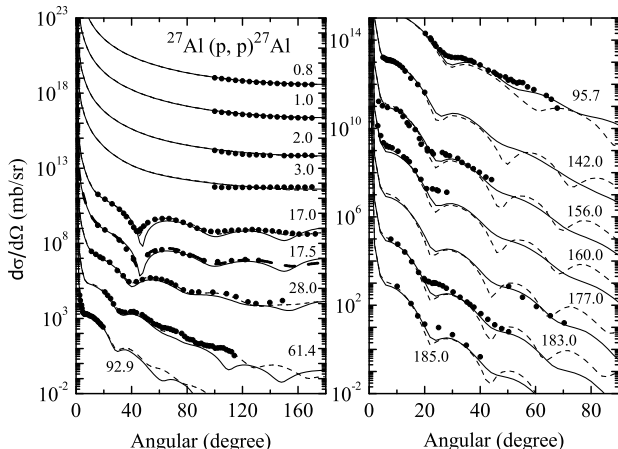


FIG. 13: Same as in Fig.12, except for  $p+^{27}\text{Al}$  elastic scattering for induced energy  $800\text{keV} < E < 185.0 \text{ MeV}$ . The experimental data are shown in Table II.

demonstrated that the isospin asymmetry has an obvious impact on the OMP potentials.

To apply this RMOP in a convenient way and make it accessible to other research groups, explicit expressions for the nucleon scalar and vector potentials might be desired. In this work, we systematically analyze the energy, density and isospin dependence of the nucleon self-energies and the Dirac potentials in nuclear matter and the Schrödinger equivalent potentials in finite nuclei. It is observed that the potential is sensitive to the isospin parameter  $\beta$ , but some features related to the energy

dependence are not sensitive to  $\beta$ . The full parameterization of this RMOP and the extensive application will be studied in the following work.

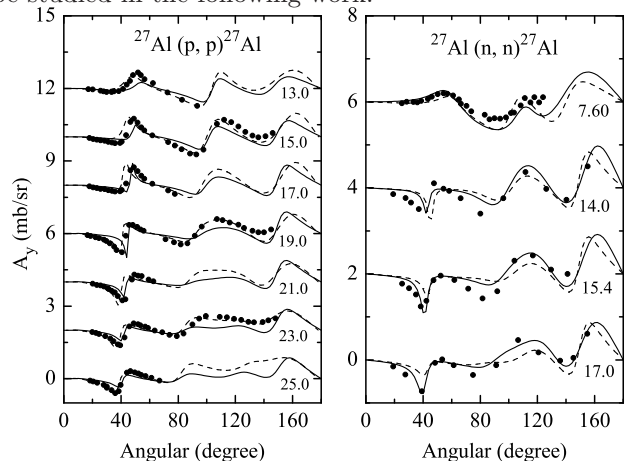


FIG. 14: Analyzing powers of  $p,n+^{27}\text{Al}$  elastic scattering. The curves and data points at the bottom represent their true values, the others are shifted by increments of 2, 4, etc. The notations are the same as in Fig. 12. The experimental data are listed in Table I-II.

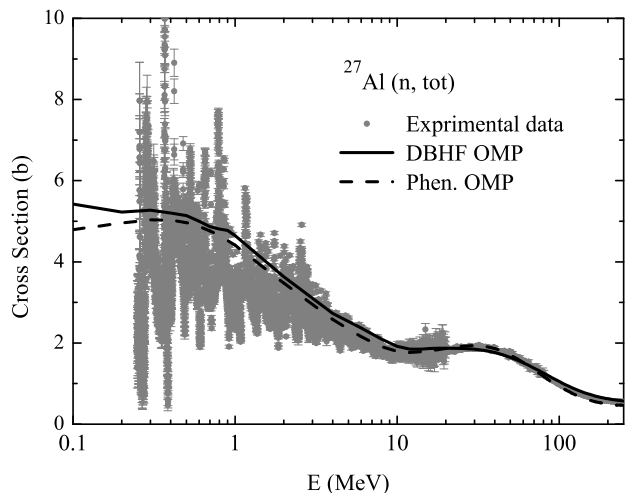


FIG. 15: The cross sections of  $n+^{27}\text{Al}(n,\text{tot})$ . The experimental data are listed in Table I. The Phenomenological OMP indicates the results calculated with the KD potentials.

### Acknowledgments

This work has been supported by the National Natural Science Foundation of China (Grant Nos. 10875150 and 11175216); the Deutsche Forschungsgemeinschaft (DFG) under contract no. Mu 705/5-2.

[1] J.P. Jeukenne, A. Lejeune, and C. Mahaux, Phys. Rev. C 16, 80 (1977).

[2] Z.Y. Ma, P. Zhu, Y.Q. Gu, and Y.Z. Zhou, Nucl. Phys.

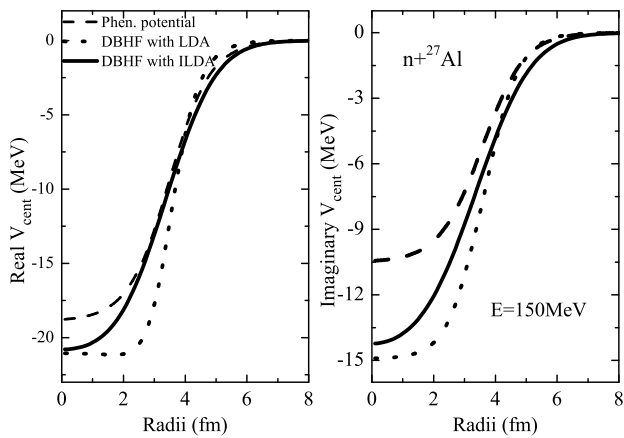


FIG. 16: The center potentials of  $n+^{27}\text{Al}$  at 150 MeV within this DBHF approach in LDA and ILDA as well as the phenomenological approach (labeled as Phen. potential in this figure).

- A 490, 619 (1988).
- [3] D. Bonatsos and H. Müther, Nucl. Phys. A 510, 55 (1990).
- [4] G.Q. Li, R. Machleidt, R. Fritz et al., Phys. Rev. C 48, 2443 (1993).
- [5] B.Q. Chen and A.D. Mackellar, Phys. Rev. C 52, 878 (1995).
- [6] J. Rong and Z.Y. Ma and N. van Giai, Phys. Rev. C 73, 014614 (2006).
- [7] Z.H. Li, U. Lombardo, H.J. Schulze et al., Phys. Rev. C 77, 034316 (2008).
- [8] Y. Han, H. Guo, and Q. Shen, Nucl. Phys. A834, 495 (2010).
- [9] W. Zuo, U. Lombardo, H.J. Schulze et al., Phys. Rev. C 74, 014317 (2006).
- [10] A. Bouyssy, J.F. Mathiot, N. van Giai et al., Phys. Rev. C 36, 380 (1987).
- [11] R. Brockmann and R. Machleidt, Phys. Rev. C 42, 1965 (1990).
- [12] F. Sammarruca and P.G. Krastev, Phys. Rev. C 75, 034315 (2007).
- [13] E.N.E. van Dalen, C.Fuchs, and Amand Faessler, Nucl. Phys. A744, 227 (2004).
- [14] E.N.E. van Dalen, C. Fuchs, and A. Faessler, Eur. Phys. J. A 31, 29 (2007).
- [15] E.N.E. van Dalen and H.Müther, Phys. Rev. C 82, 014319 (2010).
- [16] E. Schiller and H. Müther, Eur. Phys. J 11, 15 (2001).
- [17] J. S. Bell and E. J. Squires, Phys. Rev. Lett. 3, 96 (1959).
- [18] E.N.E. van Dalen and H. Müther, Int. J. Mod. Phys. E 19, 2077 (2010).
- [19] C.H. Lee, T.S. Kuo, G.Q. Li et al., Phys. Lett. B 412, 235 (1997).
- [20] S. Ulrych and H. Müther, Phys. Rev. C 56, 1788 (1997).
- [21] C. Nuppenau, Y. J. Lee, and A. D. MacKellar, Nucl. Phys. A504, 839 (1989).
- [22] T.Gross-Boelting, C.Fuchs, and Amand Faessler, Nucl. Phys. A648, 105 (1999).
- [23] Wei Zou, Yuan Tian, and Zhong-Yu Ma, Phys. Rev. C 78, 064613 (2008).
- [24] J.W.Negele, Phys. Rev. C 1, 1260 (1970).
- [25] A. Gilbert and A.G.W. Cameron, Can. J. Phys. 43, 1446 (1965).
- [26] Shen Qingbiao, Nucl. Sci. Tech. 141, 78 (2002).
- [27] A.J.Koning and J.P.Delaroche, Nucl. Phys. A 713, 231 (2003).
- [28] G.Rohr,R.Shelley, C.Nazareth, and M.Moxon, in: J.K. Dickens(Ed.), Proceedings of the International Conference on Nuclear Data for Science and Technology, Gatlinburg, 215 (1994).
- [29] R.W.Finlay, W.P.Abfalterer, G.Fink et al., Phys. Rev. C 47, 237 (1993).
- [30] D. C. Larson, J. A. Harvey, and N. W. Hill, Report of ORNL 5787, 174 (1981).
- [31] R.L.Becker, W.G.Guindon, and G.J.Smith, Nucl. Phys. 89, 154 (1966).
- [32] W.E.Kinney and F.G.Perey, Report of ORNL 10, 4516 (1970).
- [33] G.Dagge, W.Grumb, J.W.Hammer et al., Phys. Rev. C 39, 1768 (1989).
- [34] C.S.Whisnant, J.H.Dave, and C.R.Gould, Phys. Rev. C 30, 1435 (1984).
- [35] M.M.Nagadi, C.R.Howell, W.Tornow et al., Phys. Rev. C 68, 044610 (2003).
- [36] J.S.Petler, M.S.Islam, R.W.Finlay et al., Phys. Rev. C 32, 673 (1985).
- [37] A.Bratenahl,S.Fernbach, R.H. Hildebrand et al., Phys. Rev. 77, 597 (1950).
- [38] G.L. Salmon, Nucl. Phys. 21, 15 (1960).
- [39] C.P.Van Zyl, R.G.P.Voss, and R.Wilson, Philos. Mag. 1, 1003 (1956).
- [40] Ph.Martin and R.L.Walter, Phys. Rev. C 34, 384 (1986).
- [41] M.Chiari, L.Giuntini, P.A.Mando et al., Nuclear Instrum.and Methods in Physics Res. B 174, 259 (2001).
- [42] I.E.Dayton and G.Schrank, Phys. Rev. 101, 1358 (1956).
- [43] G.M.Crawley, Phys. Rev. 167, 1070 (1968).
- [44] R.Dittman, H.S.Sandhu, R.K.Cole et al., Nucl. Phys. A126, 592 (1969).
- [45] C.B.Fulmer, J.B.Ball, A.SCOTT et al., Phys. Rev. 181, 1565 (1969).
- [46] G.Gerstein, J.Niederer, and K.Strauch, Phys. Rev. 108, 427 (1957).
- [47] A.E.Taylor and E.Wood, Nucl. Phys. 25, 642 (1961).
- [48] V.Comparat, R.Frascaria, N.Marty et al., Nucl. Phys. 221, 403 (1974).
- [49] A.Johansson, G.Tibell, K.Parker et al., Nucl. Phys. 21, 383 (1960).
- [50] A.Johansson, U.Svanberg, P.E.Hodgson et al., 19, 541 (1961).
- [51] S.Dahlgren, D.Hasselgren, B.Hoistad et al., Nucl. Phys. A90, 673 (1967).
- [52] R.Roy, C.R. Lamontagne, R.J. Slobodrian et al., Nucl. Phys. A411, 1 (1983).
- [53] Z.Y.Ma and L.Liu, Phys. Rev. C 66, 024321 (2002).
- [54] D.P. Murdock and C.J. Horowitz, Phys. Rev. C 35, 1442 (1987).